RZ 1513 (#54700) 9/17/86
Physics 28 pages

FORCE SENSING IN SCANNING TUNNELING MICROSCOPY

U. DÜRIG, J.K. GIMZEWSKI, D.W. POHL and R. SCHLITTLER
IBM Zurich Research Laboratory, 8803 Rüschlkon, Switzerland

ABSTRACT: The observation of interaction forces on an atomic scale is discussed. We show that the sensitivity is essentially limited by thermal fluctuations and by instabilities which can arise for attractive interaction potentials. An experiment was designed in order to explore the forces acting between tunnel tip and sample during scanning tunneling microscopy (STM). Force gradients were detected as resonance shifts of cantilever beams used as sample stage. Beam deflections caused by force variations were also recorded. We present data for tungsten tips and polycrystalline silver surfaces prepared under UHV conditions. Large positive force gradients were found for the range of tunnel distances investigated. Force maps show pronounced features correlating directly with topographic structures.

August 7, 1986

LIMITED DISTRIBUTION NOTICE

IBM Research Division
Almaden • Yorktown • Zurich

1. Introduction

The range of applications of scanning tunneling microscopy (STM) has been constantly extended [1]. Recently, attention turned to measuring interaction forces acting between tip and sample on an atomic scale [2,3]. To date, only scant information on these local interactions is available. Such forces are of fundamental importance for the understanding of surface interactions such as adhesion and friction. Furthermore, forces between tunnel tip and sample should be considered for the interpretation of STM data particularly when soft materials are investigated. For instance, it has been proposed that the anomalously large corrugation amplitudes observed on the atomic scale on graphite (0001) surfaces can be accounted for by assuming elastic deformations of the graphite surface owing to tip-sample interaction forces [4].

Up to now, most experimental investigations of interaction forces have been carried out using the surfaces of two macroscopic objects in an approximately planar geometry [5-7]. The interaction area in these experiments is typically of the order of several μm^2, and the minimum distance and resolution are limited by residual roughness to about 10 Å. Consequently, only long-range interactions such as Van der Waals (VdW) forces averaged over a large number of atoms can be investigated.

With STM, on the other hand, a lateral resolution in the Å range is inherent. Furthermore, the gap width can be made extremely small so that short-range forces such as exchange-correlation forces or even core

repulsion forces become accessible. However, owing to the small interaction area, the resulting forces are orders of magnitude smaller than in planar geometries. Binnig et al. [2] describe a scheme which overcomes this problem by exploiting the large sensitivity of the tunnel current upon gap width to monitor sub-Å deflections of an elastic cantilever beam. The deflections were induced by an independent stylus scanned across a surface [Atomic Force Microscope (AFM)] under isodynamic conditions, i.e. using force quantities as the control parameter.

In our approach, interaction and conventional tunnel data (topography, barrier height) are *simultaneously* recorded. This permits direct correlation of both data which are complementary owing to the different physical processes involved. Our experiments will be discussed in the second part of this paper while the first section is devoted to a detailed discussion of force measurements.

2. Force measurement

Interaction forces (i.e. first derivative of the interaction potential with respect to distance dU_{int}/ds) are determined most simply by measuring deflections induced in a spring. Force gradients, d^2U_{int}/ds^2, give rise to detectable shifts in the resonance properties of the spring. Both quantities, dU_{int}/ds and d^2U_{int}/ds^2, can be measured simultaneously with one single device [6].

Typical forces between single atoms are of the order of 10^{-8} N for covalent binding, and 10^{-11} N for VdW interactions. They produce deflections of about 0.1 Å with a spring constant C = 100 ... 1 Nm^{-1}. Such displacements can be readily detected, by STM-like vacuum tunnel junctions or by interferometric means [8]. The spring constants required can be realized conveniently with thin membranes or cantilever beams.

Since sensitivity is a prime objective in an "atomic-force" sensor design, a soft spring (small C) appears desirable. However, for an attractive potential, C must be larger than the force gradient otherwise the sensor becomes unstable. Thermal vibrations of the spring impose further constraints since a force measurement on the atomic scale involves energies comparable to k_BT.

In the following analysis, the atomic-force sensor is assumed to be a damped harmonic oscillator (fig. 1a). The interaction between tip and sample is described by a potential U_{int} (s). In the extreme, U_{int} can be the interaction potential between a single atom at the very apex of the tunnel tip and a single atom of the sample.

Hamiltonian H and partition function Q of this system are [9]

$$H = H_{osc}(p,y) + U_{int}(d - y) \ , \tag{1a}$$

$$Q = \int dy\, dp\, e^{-\beta H} \ , \tag{1b}$$

where $H_{osc} = 1/2m\,p^2 + 1/2\ Cy^2$ is the Hamiltonian of the spring, $\beta = 1/k_BT$, p the momentum of mass m, and y its deflection under the influence of U_{int}. For convenience, it is assumed here that the base of the spring is fixed with respect to the sample, i.e. d = const. Without interaction ($U_{int}=0$) the tip would be in position (1). With U_{int} turned on, a new equilibrium is established, (2), with a mean deflection

$$\langle y \rangle = \frac{1}{Q} \int dy\ dp\ y\ e^{-\beta H} \qquad (2)$$

which for large β (i.e. low temperatures) is equivalent to the condition of classical force balance

$$Cy_0 - (dU_{int}/dy) = 0\ . \qquad (3)$$

y_0 is the equilibrium position without thermal vibrations. Note that $d = y + s$ is the control parameter in this analysis, while in AFM, it is $\langle y \rangle$ and in our experiment, described below, it is $\langle s \rangle$.

Expansion around y_0 yields for small $\eta \equiv y - y_0$:

$$H(p,y) = H(p,y_0) + 1/2\ C_{eff}\,\eta^2\ . \qquad (4)$$

The sample-tip-spring system hence reduces to a harmonic oscillator with a resonance frequency determined by both the spring constant and interaction force gradient,

$$C_{eff} = C + d^2U_{int}/ds^2 = m\omega_0^2 \ . \qquad (5)$$

Two independent modes of force sensing are thus possible. In a static mode, the interaction force is determined by detecting the spring deflection. This mode requires accurate length measurements on the sub-Å to Å scale. The dynamic mode, on the other hand, provides information on the force gradient from a frequency measurement which technically is easier than absolute amplitude determinations.

A rough estimate of the interfacial force can be obtained from calculations of the interaction potential w(s) (per unit area) between planar metal surfaces [10] and the so-called Derjaguin approximation [11] for slightly curved surfaces ($R > s$, cf. fig. 1b):

$$F_{int}(s) = 2\pi R w(s) \ . \qquad (6)$$

F_{int} is plotted in fig. 1c for a tip radius of 10 Å. Note that s is the distance between the two jellium edges, each of which extends about 1 Å beyond the

core position of the surface atoms. One recognizes that the force is attractive over the whole range of distances; the values for $s < 1$ Å, however, are probably not physically relevant since the jellium approximation begins to fail at such small separations.

The force exerted by the spring is represented by straight lines in fig. 1c for two different values of C. For the softer spring, $C = 5\ Nm^{-1}$ (solid line) three intersections are found for $3.5\ Å < d < 5.5\ Å$. The intersections correspond to the positions of the two minima of the total potential energy and the maximum of the energy barrier between them (fig. 1d). The system may remain in a metastable equilibrium as long as the thermal energy k_BT is not sufficient to overcome the energy barrier.

Suppose now that the soft force sensor approaches the sample surface. First, equilibrium is established corresponding to a small spring deflection. As d approaches ~ 3.5 Å, the energy barrier eventually disappears and the system makes a discontinuous transition into a new equilibrium corresponding to much larger spring deflection and closer tip-sample proximity. Upon retraction, a similar transition occurs at $d \sim 5.5$ Å. No stable equilibria exist for tip-sample separations in the range $0.7\ Å < s < 2.6\ Å$, i.e. between the points where the spring line is tangent to the force curve.

No such problems exist when a sufficiently large C is chosen ($C \sim 20\ Nm^{-1}$, dashed curves in figs. 1c and d). Optimum performance of

the force sensor, i.e. high sensitivity and stability, is achieved by operating close to the instability point.

Thermal vibrations are sizable as can be seen from the vertical bar in fig. 1d. Their mean-square amplitude is

$$\langle \eta^2 \rangle = \frac{1}{Q} \int dp\ d\eta\ \eta^2\ e^{-\beta H(p,\eta)} \ . \tag{7}$$

For sufficiently large β, higher-order terms in the expansion of U_{int} may again be neglected yielding for $\langle \eta^2 \rangle$ the equipartition value of a harmonic oscillator

$$\eta_0^2 = k_B T / C_{eff} \ . \tag{8}$$

These vibrations affect the force (force-gradient) measurement in two ways. First, anharmonic corrections must be added to expressions (3) and (5), and second, sensitivity is limited by random forces driving the vibrations.

The first-order correction to eq. (3) can be easily calculated using the series expansion of U_{int} (see Appendix A). The deviation of the true expectation value from the zero-temperature value, $\langle \eta \rangle$, amounts to

$$\langle \eta \rangle = \left(\eta_0^2 / 2C_{eff}\right) d^3 U_{int} / ds^3 \tag{9}$$

Hence, the error made in evaluating the interaction force by means of eq. (3) is

$$\delta F_{ah} = C\langle\eta\rangle = \left(\eta_0^2 C/2C_{eff}\right) d^3U_{int}/ds^3 \ . \tag{10}$$

The correction to eq. (5) owing to higher-order terms can be estimated in a similar way. To lowest order one finds

$$\delta C_{eff_{ah}} = \ - (5/16)\, \eta_0^2\, d^4U_{int}\, /ds^4 \ . \tag{11}$$

The random driving forces are connected intimately with energy dissipation [12] described by a damping factor Γ. These forces give rise to random fluctuations of phase and amplitude of the oscillatory spring motion $\eta(t)$. As a consequence, the autocorrelation function

$$g(t) = \lim_{T\to\infty} \frac{1}{2T} \int_{-T}^{T} \eta(t)\, \eta\, (t - \tau) d\tau \tag{12}$$

decays exponentially ($\Gamma << \omega_0$)

$$g(\tau) = \langle\eta^2\rangle\, e^{-\Gamma|\tau|} \cos\, \omega_0\tau \ . \tag{13}$$

In practice, only estimates of $\langle y \rangle$ can be measured within a finite time interval, e.g. using a low-pass filter with integration time t_0. The mean-square flucutations of the measured estimate

$$\langle y \rangle_{t_0} = \frac{1}{t_0} \int_0^{t_0} y(t)\, dt \tag{14}$$

can be expressed in terms of the autocorrelation function (12). Using the approximate expression (13) for $g(\tau)$ and $t_0 >> 1/\omega_0$ ($Q = \omega_0/2\Gamma$), one finds

$$\langle (\langle y \rangle_{t_0} - \langle y \rangle)^2 \rangle = 2\langle \eta^2 \rangle / Q\omega_0 t_0 \ . \tag{15}$$

Thus, the thermal-noise limit of the force measurement becomes

$$\delta F_{th} = (2C_{eff}\, k_B T/Q\omega_0 t_0)^{1/2} \ . \tag{16}$$

Additional insight is gained by treating the thermal-noise problem in the frequency domain. The force sensor is a linear device with transfer function

$$g(\omega) = C_{eff}^{-1}\, \omega_0^2 / \left(\omega^2 - \omega_0^2 + 2i\Gamma\omega\right) \tag{17}$$

relating deflections $y(\omega)$ to driving forces $F(\omega)$ comprising both interaction and random forces. Assuming a white-noise spectrum of the random forces $F_r(\omega)$ [13], and using the identity $\langle \eta(\omega)\eta^*(\omega)\rangle = k_B T/C_{eff}$, one obtains

$$F_r F_r^* = 2\, C_{eff}\, k_B T/Q\omega_0 \ . \tag{18}$$

In order to be detectable, interaction forces must be at least of the same magnitude as the random force $(F_r F_r^*\, \Delta\omega)^{1/2}$, where $\Delta\omega$ is the bandwidth of the measurement. Eq. (16) represents the detection threshold for unit signal-to-noise ratio. The amplitude response of a force sensor can be greatly enhanced by operating it in a resonant mode [2]. However, this scheme does not improve the detection limit set by thermal noise since the response of both random and interaction forces is amplified.

The detection threshold for C_{eff} is governed by fluctuations, δE, of the vibrational energy $E = C_{eff}\langle \eta^2 \rangle$. These energy fluctuations, arising from random forces, have an rms amplitude of approximately ($\Gamma << \omega_0$)

$$\delta E = 2\eta_0 (F_r F_r^*\, \Delta\omega)^{1/2} \ . \tag{19}$$

With $\delta E = \delta C_{eff}\, \eta_0^2$, one finds that $\delta C_{eff_{th}} = C_{eff}\, \delta E/E$ is proportional to the relative energy fluctuation. Since δE is proportional to $E^{1/2}$, $\delta C_{eff_{th}}$ can be improved by externally pumping the spring resonator, e.g. by means of additional feedback, in order to increase the stored vibrational energy. The

amount of feedback that can be applied is limited only by the maximum vibration amplitude η_0 that will not disturb the measurement.

In an actual force sensor, a flexible cantilever beam or a membrane typically acts as a spring. These mechanical devices have an infinite number of eigenmodes each contributing to the thermal vibrations. The partition function of the system can be written as

$$Q = \int da_0 \ldots da_n \quad \exp\left[- \beta \sum_n H(a_n \Psi_n)\right] , \tag{20}$$

where the Ψ_n represent the normalized eigenmodes of the total Hamiltonian. Except for Ψ_0 corresponding to a static deflection, H will again have the form of a harmonic oscillator if terms of order higher than 2 in U_{int} are neglected.

In the following, we consider a cantilever beam (CB) rigidly clamped at one end (fig. 2). We are concerned with bending vibrations along the y-axis only. Fig. 2b shows the relative deflections $\Psi_i(x)$ for a free beam ($U_{int} = 0$) in thermal equilibrium, i.e. each mode has an energy k_BT. The vibration amplitude at the unclamped end rapidly decreases with n. In fact, since ω_0^2 is roughly proportional to $1/n^4$, $\Psi_n(\ell)$ decreases as $1/n^2$. The only relevant contribution therefore comes from the first eigenmode.

The equations derived for the spring force sensor can be readily adapted to the cantilever beam. We restrict ourselves to the limit $|d^2U_{int}/ds^2| << C$. The static force constant of the beam, C, is determined from $C\Psi_0(\ell) = F$, where $\Psi_0(\ell)$ is the deflection owing to a point force F acting on the free

end. The exact analogues to eqs. (5) and (8) are rather involved. In our approximation, however, one obtains expressions which only slightly deviate from the ones for a spring, namely

$$m_{eff}\ \omega_1^2 = C + 0.97\ (d^2U_{int}/ds^2) \equiv C^*_{eff}\ , \tag{21}$$

and

$$\eta^2 \equiv \langle \Psi_1^2(\ell) \rangle = k_BT/1.03\ C^*_{eff}\ . \tag{22}$$

m_{eff}, approximately 0.24 times the cantilever mass, is defined by $m_{eff}\,\omega_1^2 = C$.

The performance of a CB sensor thus can be calculated using the equations previously derived. For example, a beam with a force constant $C = 20\ Nm^{-1}$ (see fig. 1, dashed curves) yields a detection threshold of 1.3 pN at room temperature, $\omega_1 = 1$ kHz, $Q = 100$ and a detection bandwidth of 1 Hz. The corresponding value for the force-gradient measurement amounts to $0.18\ Nm^{-1}$. These values are well below the respective values of our estimate for the metallic tip-sample interaction.

3. Experiment

The interaction between tip and sample surface in the STM was investigated using a flexible CB as sample holder. In these experiments, the tip of a normal STM is used both for tunneling and as a force probe permitting high-resolution mapping of forces (force gradients) simultaneously with conventional STM images. The tip is scanned using the tunnel-gap spacing s as a control parameter which can be readily adjusted by the tunnel parameters (barrier height, current and voltage). Force maps obtained in this way can be correlated direct to surface data obtained in STM.

The experiments were conducted with a "pocket-size" STM [14] mounted in a UHV chamber ($p \leq 2 \times 10^{-10}$ mb) equipped with a sample preparation chamber and transfer device. The sample substrates were thin CB's made of copper and steel. Thick silver films ($\sim$ 2000 Å) were condensed on the CB's, at $T = 300$ K, $p \simeq 10^{-9}$ mb in the preparation chamber, and transferred to the STM chamber under UHV conditions. STM measurements were conducted using an in-situ sputtered W-tip sharpened by operating it in the field-emission mode with a separate sample as anode.

Theoretical calculations of intermetallic adhesion forces [10] predict attractive tip-sample forces of the order of nN, and force gradients of the order of Nm^{-1} under typical tunnel conditions (fig. 1c). Accordingly, an elastic compliance (measured at the free end of the CB) of 2 Nm^{-1} and 10 Nm^{-1} was chosen as a design parameter for the copper and steel

beams, respectively. The actual dimensions of the beams were adjusted such that a resonance frequency of a few hundred Hz was obtained. The mechanical properties of the beams are summarized in table 1. Using eq. (8), the estimated thermal vibration amplitude is of the order of 0.2 ... 0.5Å. Such vibrations can be readily detected as a modulation in the tunnel current.

In a first set of experiments, we concentrated upon the *spectrum of the current* I_t. Fig. 3 shows two typical spectra measured with the tunnel tip near the end of the steel CB; S(ν) is the power density of ln (I_t) calibrated to the amplitude of the reference peak (see below). The spectra were measured sequentially at I_t = 2 nA, and V_t = 1.5 and 0.45 V, respectively. The thermal excitation of the CB manifests itself as a broad peak around 650 Hz (830 Hz). The spikes are caused by residual vibrations and harmonics of line frequency pick-up. However, the 1200 Hz peak, is a control signal produced by modulation of the tip-sample gap width with an amplitude of 0.06 Å. This modulation was used to calibrate the spectrum and to determine the tunnel barrier height ($\Phi \simeq$ 2-3 eV) by phase sensitive detection.

Comparison of the two spectra in fig. 3 and other spectra consistently shows a positive frequency shift which increases when going to higher tunnel currents or lower voltages. From these observations, we conclude that the force gradient is positive and that it increases as the tip gets closer to the sample surface.

The measured frequency shifts $\Delta\nu_R$ exhibit a systematic increase as a function of position x_{tip} along the beam length. Fig. 4 shows, for Ag surfaces, experimental values for the two beams.

The observed increase of ν_R versus x_{tip} is a consequence of the decrease of static spring constant $C(x_{tip})$, hence increase of $C_i/C(x_{tip})$ along the CB ($x_{tip} = 0...\ell$).

Owing to the large frequency shifts, eq. (21) cannot be employed to determine the interaction force gradient C_i. Instead, $\nu_R(x_{tip})$ was calculated leaving C_i as a fit parameter (see Appendix B). A best fit of C_i = 15 and 50 Nm^{-1} was obtained for both beams.

We also measured the rms vibration amplitude by integrating the spectra in fig. 3 to check consistency with thermal excitation. For this purpose, the peaks were approximated by smooth curves discarding sharp spikes and the background level. The resulting values of 0.19 ± 0.02 Å and 0.13 ± 0.02 Å for the 650 Hz and 830 Hz peaks, respectively, compare reasonably well with the thermal equilibrium values of 0.16 Å and 0.12 Å obtained from calculations taking into account the force gradient between tip and sample determined from the frequency shift.

The measured resonance frequencies exhibit considerable scatter. We suspected that this was caused by local variations of the interaction potential on the sample surface and unavoidable drift in lateral position during data acquisition. To substantiate this idea, we took a series of STM images for different positions x_{tip} and values I_t, V_t (fig. 5). Above the base ($x_{tip} = 0$,

fig. 5a), the position z_{tip} recorded in these scan images represents the topography of the surface in the usual way; individual crystallites with facets gently inclined towards each other separated by compact boundaries are clearly resolved. The topography closely resembles that previously reported for Ag films condensed at 300 K [15]. Above the free part of the CB, however, the value of z_{tip} is expected to be a superposition of topography and CB deflection at constant gap spacing.

Figs. 5b-d were obtained at $x_{tip} = \ell$ for three different values of V_t on the same image area. The grooving between the flat areas and grain boundaries increase dramatically when lowering V_t from 1.4 to 0.063 V. No such increase in apparent grooving could be found for the same variation of V_t on the fixed base region. We conclude that the apparent increase in grooving is caused by a strong change of forces in the vicinity of the silver grain boundaries. Fig. 4d showing the largest grooving hence is essentially a *force map* of the surface with an estimated lateral resolution of $\sim$ 10 Å.

Fig. 5c shows the typical change of this additional force as a function of tunnel voltage. From knowledge of the tunnel parameters and the barrier height measured, the approximate scale on the top of the plot was determined using $\Delta s \approx (\Delta \ln V_t) / A\Phi^{1/2}$ ($A \sim 1$ Å^{-1}eV$^{-1/2}$).

The absolute tunnel gap cannot be experimentally determined here. However, typical values of 5-10 Å are expected from tunnel theory [16]. One recognizes very similar behavior at the three sites with a force swing as large as 10 nN. The slope of the curves yields a compliance between 30 and

100 Nm^{-1} which is consistent with the above frequency-shift analysis. STM scans repeated at different positions, on different CB's, and with various values of I_t and V_t showed similar pseudo-topographic features.

4. Discussion

Calculations based on a jellium model of the interaction between two metals [10] consistently predict attractive potentials with a minimum near one lattice constant, and a depth comparable to the binding energy. The force gradients derived from these calculations, normalized to the area covered by one surface atom (approx. 3 × 3 $Å^2$), are of the order of -0.1 ... -0.5 Nm^{-1} at distances s of several Angstrom. They change sign at approximately 1.5 Å reaching values of about 5 Nm^{-1} near the potential minimum.

The force gradients C_i found in our experiments have values in between +15 and +50 Nm^{-1}. To interpret this result in terms of the above estimates, a tip-sample (jellium edge) distance $s < 1.5$ Å and an interaction area of about 10 × 10 $Å^2$ are required. While the latter requirement appears reasonable, the first leads to a vanishing barrier height resulting in a low-resistance metallic point contact. This is in clear contradiction to the tunnel characteristics observed, viz. $\varphi \sim 3$ eV and $R_T \sim 10$ MΩ ... 1000 MΩ. Whether additional contributions to the interaction potential or a difference in the effective gap spacings for force and tunneling interactions are responsible for the discrepancy observed cannot be resolved at the present stage.

The change observed in the interaction force at grain boundaries could be accounted for by an increase of the effective interaction area as the tip dives into a valley formed by two adjacent silver grains. This implies a corresponding increase of C at grain boundaries consistent with our data. Furthermore, one then may conclude that the interaction force is repulsive in our experiments. On the basis of this model, a pressure of $\sim$ 1 GPa at the tip apex can be estimated. Such pressures are close to the macroscopic deformation limit. The respective microscopic limit is considerably larger [5], indeed we detected no topographic changes induced by repetitive scanning. Soler *et al.* [4] recently pointed out that the interactive forces can induce significant deformations for soft material surfaces. In our case, however, the elastic deformations calculated amount to less than 0.1 Å.

5. Conclusions

Measuring interactive forces on an atomic scale requires careful design of the sensor, in particular with regard to instabilities induced by attractive potentials and to the effect of thermal vibrations. Our experimental results show that force and topographic components can be simultaneously monitored. The shift in beam resonance frequency is sensitive to the local force gradient only, whereas the "topography" measured is a combination of the surface profile as seen by regular STM and local force variations. Their relative contributions are determined by the chosen force constant of the sensor spring.

Acknowledgements

It is a pleasure to acknowledge useful discussions with H. Rohrer, K. H. Rieder, and R. Horn. We thank A. Brunner for his computational help, and H. Meier for technical assistance.

Appendix A: Anharmonic Corrections

First, the expectation value $\langle \eta \rangle = \langle y \rangle - y_0$ is calculated using the series expansion

$$H = H(p, y_0) + \frac{1}{2} C_{eff} \eta^2 + \sum_{n=3} \frac{(-1)^n}{n!} \frac{d^n U_{int}}{ds^n} \eta^n \tag{A1}$$

in equation (2) ($C_{eff} = C + d^2U_{int}/ds^2$):

$$\langle \eta \rangle = \frac{1}{Q} \int dp\, d\eta\ \eta\ \exp\left\{-\beta\left[H(p,y_0) + 1/2\ C_{eff}\eta^2\right]\right\} \cdot \exp\left\{-\beta\left(\sum_{n=3} \frac{(-1)^n}{n!} \frac{d^n U_{int}}{ds^n} \eta^n\right)\right\} . \tag{A2}$$

Expanding the second exponential to first order in $\beta(\sum_{n=3} \ldots)$, one obtains

$$\langle \eta \rangle = \frac{1}{Q} \int dp\, d\eta\ \eta\ e^{-\beta(H(p,y_0)+1/2C_{eff}\eta^2)} - \frac{\beta}{Q} \int dp\, d\eta\, \eta \sum_{n=3} \frac{(-1)^n}{n!} \frac{d^n U_{int}}{ds^n} \eta^n\ e^{-\beta\left(H(p,y_0)+1/2\ C_{eff}\eta^2\right)} . \tag{A3}$$

The only nonvanishing contributions in (A3) stem from terms containing odd derivatives d^nU_{int}/ds^n. Neglecting derivatives with $n > 3$ one arrives at eq. (9).

In order to estimate the anharmonic correction to eq. (5), one starts from the expression for the kinetic energy of the system

$$E_{kin} = 1/2\ m\omega_0^2\langle\eta^2\rangle = 1/2k_BT\ . \tag{A4}$$

Comparison of eq. (A4) with eqs. (8) and (5) yields

$$\delta C_{eff_{ah}} = C_{eff}\left(\langle\eta^2\rangle - \eta_0^2\right)/\eta_0^2\ . \tag{A5}$$

Using the same approximations in evaluating $\langle\eta^2\rangle$ as above, one finds eq. (11).

Appendix B: Calculation of the Resonance Frequency of a Spring-Loaded CB

The equation of motion of a spring-loaded CB (see inset to fig. 4) may be written as [17]

$$EI\ \frac{\partial^4\Psi(x,t)}{\partial x^4} + \tau\ \frac{\partial^2\Psi(x,t)}{\partial t^2} = -C_i\Psi(x,t)\,\delta(x - x_{tip})\ , \tag{B1}$$

where E is the elastic modulus, I the moment of inertia, and τ the mass per unit length. The appropriate boundary conditions (i.e. clamped end at $x=0$ and free end at $x=\ell$) are

$$\begin{aligned} \Psi(x,t) = \frac{\partial\Psi(x,t)}{\partial x} &= 0 \qquad x = 0 \\ \frac{\partial^2\Psi(x,t)}{\delta x^2} = \frac{\partial^3\Psi(x,t)}{\partial x^3} &= 0 \qquad x = \ell\ . \end{aligned} \tag{B2}$$

With a harmonic ansatz, $\Psi(x,t) = e^{i\omega t}\phi(x)$ (B1) becomes

$$EI\,\frac{\delta^4\phi}{\delta x^4} - \tau\omega^2\phi = -C_i\,\phi\delta(x - x_{tip})\ . \tag{B3}$$

The solution to (B3) satisfying (B2) is of the form

$$\phi(x) = \begin{cases} A(\cos \kappa x - \cosh \kappa x) + B(\sin \kappa x - \sinh \kappa x) & x < x_{tip} \\ C(\cos \kappa x' + \cosh \kappa x') + D(\sin \kappa x' + \sinh \kappa x') & x > x_{tip} \end{cases} \qquad \text{(B4)}$$

where $\kappa^4 = \tau\omega^2/EI$ and $x' = x - \ell$. The corresponding boundary conditions at $x = x_{tip}$ are

$$\begin{aligned} &\phi,\ \frac{\delta\phi}{\delta x},\ \frac{\delta^2\phi}{\delta x^2} \quad \text{continuous} \\ &\lim_{\varepsilon \to 0} \left(\frac{\delta^3\phi(x_{tip} - \varepsilon)}{\delta x^3} - \frac{\delta^3\phi(x_{tip} + \varepsilon)}{\delta x^3} \right) = -\frac{C_i}{EI}\phi(x_{tip}) \ . \end{aligned} \qquad \text{(B5)}$$

In order to find the eigenmodes Ψ_n, and eigenfrequencies ω_n, one has to determine κ such that a nontrivial solution of the form (B4) satisfying (B5) is found. This problem was solved numerically.

References

[1] See, e.g. G. Binnig and H. Rohrer, IBM J. Res. Develop. 30 (1986) 355.

[2] G. Binnig, C.F. Quate, and Ch. Gerber, Phys. Rev. Lett. 56, (1986) 930.

[3] U. Dürig, J.K. Gimzewski, and D.W. Pohl, Phys. Rev. Lett., in press.

[4] J. Soler, A.M. Baro, N. Garcia, and H. Rohrer, Phys. Rev. Lett., in press.

[5] D. Tabor, in: Surface Physics of Materials, chap. 10, vol. 2; Ed. J.M. Blakely (Academic, New York, 1975), D. H. Buchley, J. Colloids Interface Sci. 58, (1977) 36.

[6] J.N. Israelachvili and D. Tabor, Proc. R. Soc. London, Ser. A 331, (1972) 19.

[7] M.D. Pashley and J.B. Pethica, J. Vac. Sci. Technol. A3, (1985) 757.

[8] R.M. de la Rue, R.F. Humphryes, I.M. Mason, and E.A. Ash, Proc. IEEE 119, (1972) 117.

[9] See, e.g. R.P. Feynman, in: Frontiers in Physics: Statistical Mechanics, Ed. D. Pines (Benjamin, Reading Massachusetts, 1972).

[10] J. Ferrante and J. R. Smith, Phys. Rev. B, 31, (1985) 3427.

[11] J.N. Israelachvili, in: Intermolecular and Surface Forces, Chap. 10, (Academic Press, London, 1985).

[12] H.B. Callen and T.A. Welton, Phys. Rev. 83, (1951) 34.

[13] H. Haken, in: Synergetics an Introduction, 2nd Edition, chap. 6, (Springer, Heidelberg, 1978).

[14] Ch. Gerber, G. Binnig, H. Fuchs, O. Marti, and H. Rohrer, Rev. Sci. Instrum. 57, (1986) 221.

[15] J.K. Gimzewski, A. Humbert, J.G. Bednorz, and B. Reihl, Phys. Rev. Lett. 55, (1985) 951; A. Humbert, J.K. Gimzewski, and B. Reihl, Phys. Rev. B (Rapid Commun.) 32, (1985) 4252; J.K. Gimzewski and A. Humbert, IBM J. Res. Develop. (1986) in press.

[16] J. Tersoff and D.R. Hamann, Phys. Rev. Lett. 50, (1983) 1998; A. Baratoff, Physica 127B, (1984) 143.

[17] L.D. Landau and E.M. Lifschitz, in: Elastizitätstheorie, Chap. 25, 4th Edition, (Akademie Verlag, Berlin 1975).

Table 1. Mechanical properties and dimensions of the cantilever beams used in the experiment.

	Length [mm]	Width [mm]	Thickness [mm]	C [Nm^{-1}]	ν_1 [Hz]
Copper beam	5.8	1.15	0.02	1	280
Steel beam	10.0	1.5	0.05	10	415

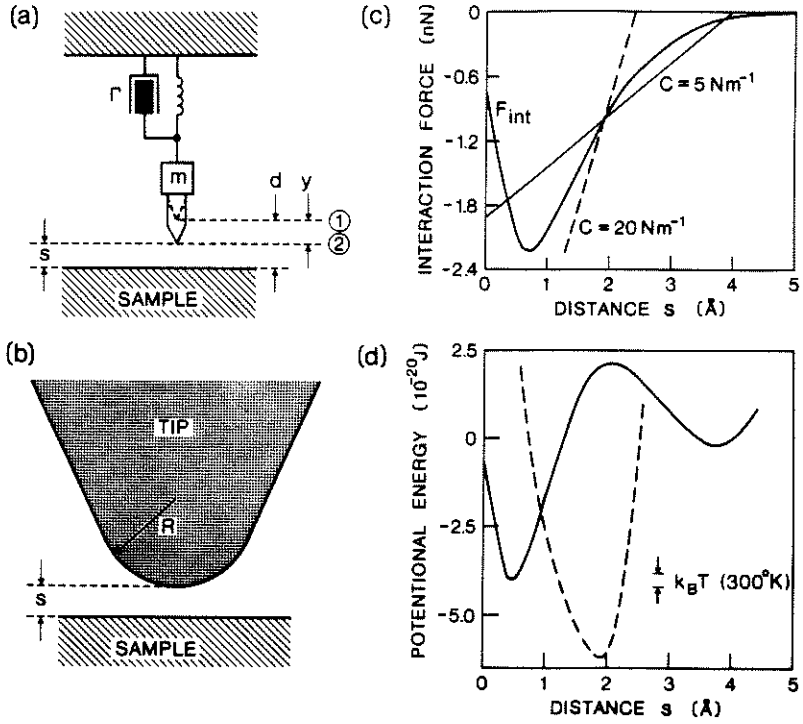

Fig. 1. (a) Schematic representation of a force sensor; (b) tip-sample geometry used to determine the adhesive interaction force; (c) interfacial and spring forces in the tip/sample system; (d) potential energy 1/2 $Cy^2 + U_{int}(s)$ of the spring-tip-sample system corresponding to (c).

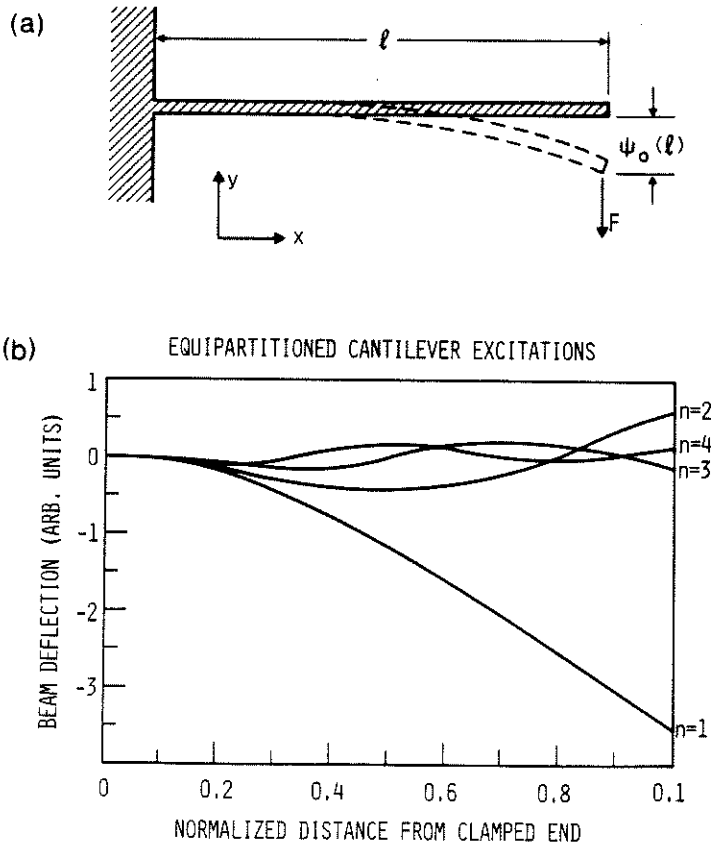

Fig. 2. Static deflection (a) and vibrational modes in thermal equilibrium (b) of a cantilever beam.

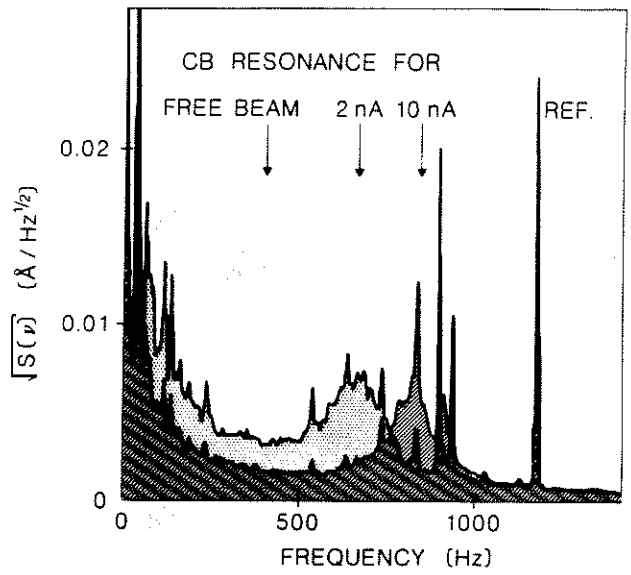

Fig. 3. Spectra of the tunnel current for I_t = 2 nA (dotted) and 10 nA (hatched) at V_t = 0.45 V. © 1986 The American Physical Society. From Ref. [3].

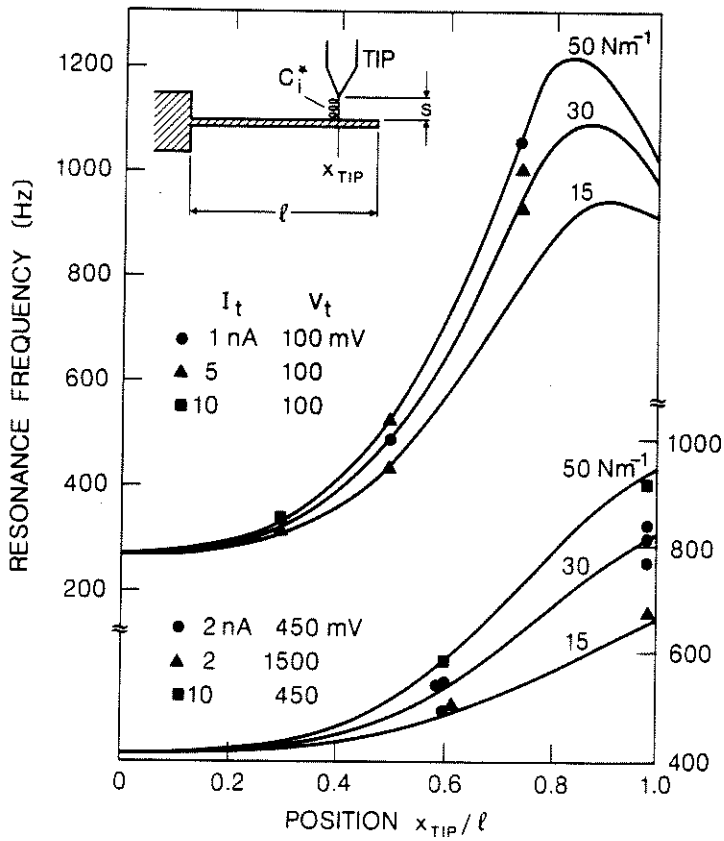

Fig. 4. Experimental and calculated CB resonance frequencies for various positions of the tunnel tip. Upper family of curves for the copper, lower one for the steel beam. © 1986 The American Physical Society. From Ref. [3].

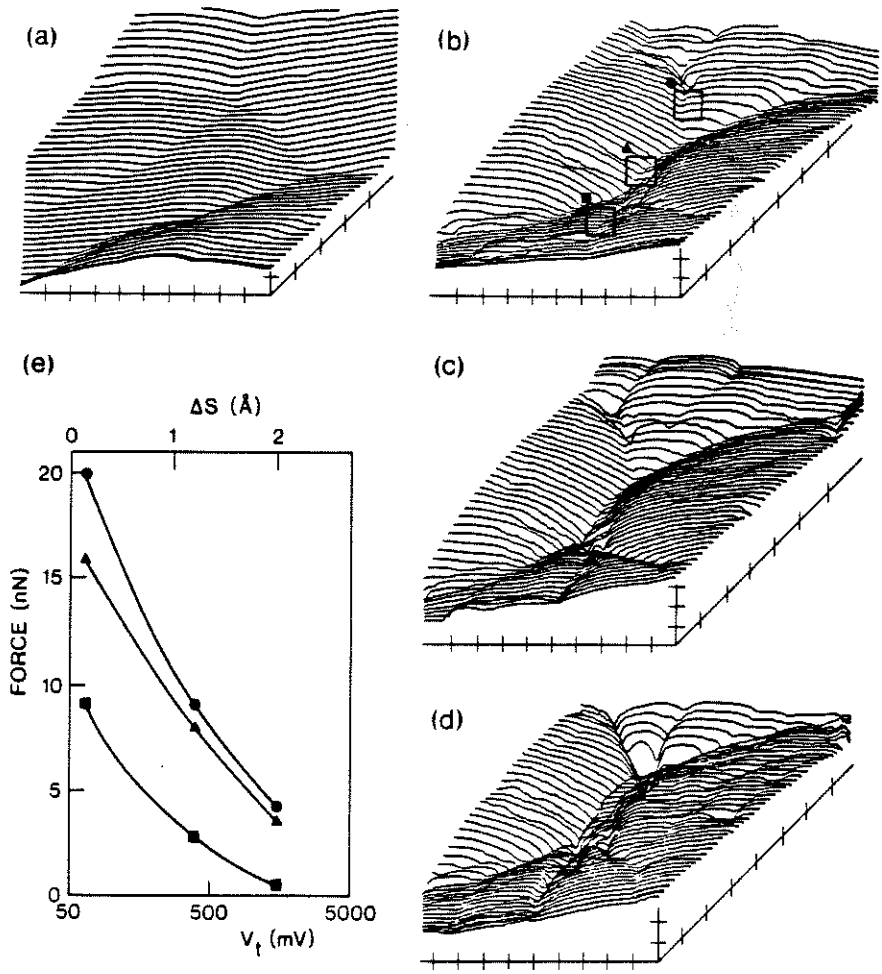

Fig. 5. STM graphs of polycrystalline Ag at the base (a) and at the free end with V_t = 1.4 (b), 0.45 (c), and 0.063 V (d). Tick marks correspond to 50 Å. (e) Force variations as a function of V_t for the three sites indicated in part (b). The curves are a visual guide only. © 1986 The American Physical Society. From Ref. [3].